ALK Molecular Phenotype in Non–Small Cell Lung Cancer: CT Radiogenomic Characterization[1]

Shota Yamamoto, MD
Ronald L. Korn, MD, PhD
Rahmi Oklu, MD, PhD
Christopher Migdal, BS
Michael B. Gotway, MD
Glen J. Weiss, MD, MBA
A. John Iafrate, MD, PhD
Dong-Wan Kim, MD, PhD
Michael D. Kuo, MD

Purpose: To present a radiogenomic computed tomographic (CT) characterization of anaplastic lymphoma kinase (*ALK*)-rearranged non–small cell lung cancer (NSCLC) *(ALK+)*.

Materials and Methods: In this HIPAA-compliant institutional review board–approved retrospective study, CT studies, *ALK* status, and clinical-pathologic data in 172 patients with NSCLC from three institutions were analyzed. A screen of 24 CT image traits was performed in a training set of 59 patients, followed by random forest variable selection incorporating 24 CT traits plus six clinical-pathologic covariates to identify a radiogenomic predictor of *ALK*+ status. This predictor was then validated in an independent cohort (n = 113). Test-for-accuracy and subset analyses were performed. A similar analysis was performed to identify a biomarker associated with shorter progression-free survival (PFS) after therapy with the *ALK* inhibitor crizotinib.

Results: *ALK*+ status was associated with central tumor location, absence of pleural tail, and large pleural effusion. An *ALK*+ radiogenomic CT status biomarker consisting of these three imaging traits with patient age of younger than 60 years showed strong discriminatory power for *ALK*+ status, with a sensitivity of 83.3% (15 of 18), a specificity of 77.9% (74 of 95), and an accuracy of 78.8% (89 of 113) in independent testing. The discriminatory power was particularly strong in patients with operable disease (stage IIIA or lower), with a sensitivity of 100.0% (five of five), a specificity of 88.1% (37 of 42), and an accuracy of 89.4% (42 of 47). Tumors with a disorganized vessel pattern had a shorter PFS with crizotinib therapy than tumors without this trait (11.4 vs 20.2 months, P = .041).

Conclusion: *ALK*+ NSCLC has distinct characteristics at CT imaging that, when combined with clinical covariates, discriminate *ALK*+ from non-*ALK* tumors and can potentially identify patients with a shorter durable response to crizotinib.

Online supplemental material is available for this article.

[1] From the Department of Radiological Sciences, David Geffen School of Medicine at UCLA, 10833 Le Conte Ave, Box 951721, CHS 17-135, Los Angeles, CA 90095-1721 (S.Y., C.M., M.D.K.); Scottsdale Medical Imaging, Scottsdale, Ariz (R.L.K.); Scottsdale Healthcare, Scottsdale, Ariz (R.L.K.); Departments of Vascular Interventional Radiology (R.O.) and Pathology (A.J.I.), Massachusetts General Hospital, Harvard Medical School, Boston, Mass; Department of Radiology, Mayo Clinic, Phoenix, Ariz (M.B.G.); Department of Radiology, Mayo Clinic, Scottsdale, Ariz (M.B.G.); Cancer Treatment Centers of America, Goodyear, Ariz (G.J.W.); Translational Genomics Research Institute, Phoenix, Ariz (G.J.W.); and Department of Internal Medicine, Seoul National University Hospital, Seoul, Republic of Korea (D.W.K.). Received April 2, 2014; revision requested April 14; revision received April 28; accepted May 1; final version accepted May 12. **Address correspondence to** M.D.K. (e-mail: *michaelkuo@mednet.ucla.edu*).

The recent identification of activating mutations and translocations in the anaplastic lymphoma kinase *(ALK)* gene in non–small cell lung cancer (NSCLC) represents an important breakthrough in lung cancer management (1–5). We now appreciate that NSCLCs harboring activation of the *ALK* gene (commonly reported as *EML4-ALK* translocation) represent a distinct lung cancer molecular phenotype (6,7). Furthermore, *ALK*, a member of the tyrosine kinase family, has recently been validated as a viable therapeutic target; patients with advanced *ALK*-rearranged *(ALK+)* NSCLC demonstrate a striking benefit in response to the small-molecule *ALK* inhibitor crizotinib (Xalkori; Pfizer, New York, NY) (4,8,9). These and similar findings in other cancers confirm the thesis that patient outcomes can be markedly improved through judicious identification and selection of patients with tumors harboring specific mutated pathways and by subsequently targeting those mutant pathways directly (10–20). Accordingly, phenotypic characterization to optimize patient stratification is becoming of paramount clinical relevance.

It is now appreciated that *ALK*+ tumors represent up to 5% of all primary NSCLCs and tend to occur in younger nonsmoking patients who have a history of never having smoked or of being former light smokers (≤10 pack-years). These tumors are predominantly of the adenocarcinoma cell type (3). Unfortunately, owing to its relatively recent discovery and low prevalence, little is known regarding the tumors' imaging characteristics and their relationship to the *ALK*+ molecular phenotype (ie, the *ALK* radiophenotype). Clearly, noninvasive imaging strategies that can aid in the identification of this molecular phenotype and its differentiation from other adenocarcinomas would be of great clinical importance. This type of analysis has been shown to be feasible in other tumors in previous studies (15,17–19,21). To address this critical need, we undertook a study to characterize the computed tomographic (CT) *ALK* radiophenotype in a multi-institutional cohort of patients with *ALK*+ disease pooled from two prospective clinical trials. Because *ALK*+ NSCLC represents a distinct and treatable molecular phenotype, our objective was to provide a radiogenomic CT characterization of *ALK*-rearranged NSCLC (*ALK*+ NSCLC) from data in a multi-institutional cohort.

Advances in Knowledge

- Anaplastic lymphoma kinase–positive *(ALK+)* tumors appear to possess a distinctive CT radiophenotype characterized by central location, absence of pleural tails, and association with large pleural effusions.
- The *ALK* radiogenomic CT status (ARCS) biomarker, an *ALK*+ status biomarker, has an accuracy of 78.8% (89 of 113), a sensitivity of 83.3% (15 of 18), and a specificity of 79.9% (74 of 95) for *ALK*+ detection in an independent validation set.
- The ARCS biomarker is particularly strong in nonadvanced disease (stage IIIA or lower), with an accuracy of 89.4% (42 of 47), a sensitivity of 100.0% (five of five), and a specificity of 88.1% (37 of 42).
- The disorganized tumor vascular pattern radiophenotype can predict patients with *ALK*+ non–small cell lung cancer (NSCLC) who are likely to have a shorter durable response to crizotinib (P = .041).

Materials and Methods

Patients and Data Selection

The institutional review boards at each of the participating centers (Seoul National University Hospital [SNUH], Massachusetts General Hospital [MGH], and Scottsdale Healthcare Medical Center [SHC]) approved this Health Insurance Portability and Accountability Act–compliant retrospective study of prospectively collected data. Only those patients who satisfied the inclusion criteria of having undergone an evaluable pretreatment enhanced chest CT study of the primary tumor or a dominant lesion and having a cell type diagnosis, clinical follow-up data, and data on *ALK* rearrangement status were included in this study (11,22,23).

All patients with *ALK*+ disease were obtained from either a phase I or a phase II multi-institutional single-arm study for the evaluation of crizotinib in patients with *ALK*+ tumors (NCT00585195 or NCT00932451, respectively) or a phase III dual-arm trial comparing crizotinib with chemotherapy in *ALK*+ tumors (NCT00932893) (11,22,23). From an initial screen of 82 patients with *ALK*+ NSCLC enrolled in the phase I, II, or III studies,

Implication for Patient Care

- *ALK*+ NSCLC has distinct characteristics at CT that, when combined with clinical covariates, discriminate *ALK*+ from non-*ALK* tumors and can potentially identify patients with a shorter durable response to crizotinib.

Published online before print
10.1148/radiol.14140789 **Content codes:** CH OI

Radiology 2014; 272:568–576

Abbreviations:
ALK = anaplastic lymphoma kinase
ARCS = *ALK* radiogenomic CT status
EGFR = epidermal growth factor receptor
KRAS = V-Ki-ras2 Kirsten rat sarcoma viral oncogene homolog
MGH = Massachusetts General Hospital
NSCLC = non–small cell lung cancer
PFS = progression-free survival
SHC = Scottsdale Healthcare Medical Center
SNUH = Seoul National University Hospital
TP53 = tumor protein 53

Author contributions:
Guarantors of integrity of entire study, S.Y., R.L.K., C.M., M.D.K.; study concepts/study design or data acquisition or data analysis/interpretation, all authors; manuscript drafting or manuscript revision for important intellectual content, all authors; manuscript final version approval, all authors; agrees to ensure any questions related to the work are appropriately resolved, all authors; literature research, S.Y., R.L.K., C.M., M.B.G., M.D.K.; clinical studies, R.O., G.J.W., D.W.K., M.D.K.; experimental studies, S.Y., R.O., M.B.G., A.J.I., M.D.K.; statistical analysis, S.Y., C.M., A.J.I., M.D.K.; and manuscript editing, all authors

Conflicts of interest are listed at the end of this article.

47 met the criteria. Thirty-seven patients came from SNUH, and 10 came from MGH. For the nonrearranged *(ALK−)* tumors, a total of 125 patients satisfied the inclusion criteria (74 from SNUH, 24 from MGH, and 27 from SHC). Detailed patient characteristics of the study population are described in Table 1.

Clinical and pathologic data were obtained from medical records, including sex, smoking status, age at diagnosis, tumor stage, cell type, *ALK*+ status, treatment regimens, objective response, and progression-free survival (PFS). Treatment responses were classified by using the standard Response Evaluation Criteria in Solid Tumors, or RECIST, 1.1 (24). PFS was measured from the 1st day of treatment until death, radiologic or clinical progression, or last follow-up.

Histologic Evaluation and Molecular Analysis

For histologic evaluation, tumors were classified by using standard World Health Organization criteria (25). Molecular analysis for *ALK*+ status was performed on formalin-fixed paraffin-embedded (FFPE) tumor samples by means of fluorescence in situ hybridization with the use of an *ALK* break-apart (or split-signal) probe, as previously described (3,11). The remaining sample types were chosen to represent a heterogeneous mix of NSCLC molecular phenotypes, reflective of the predominant adenocarcinoma mutant subtypes found in the NSCLC general population. *EGFR* (mutant/wild type), *KRAS*, and *TP53* (tumor protein 53) mutations were measured from FFPE samples by means of direct DNA sequencing (3,26).

CT Imaging Screen

Only patients who underwent pretreatment CT imaging for staging performed up to 3 months prior to treatment were included (data collected from March 2009 to February 2013). At the three institutions, enhanced chest CT was performed by using one of four CT systems (LightSpeed Ultra, GE Medical Systems, Milwaukee, Wis; Sensation 16, Siemens Medical Systems, Erlangen, Germany; or Brilliance 64 or MX8000, Philips Medical Systems, Best, the Netherlands). CT parameters were as follows: 50–150 mL of nonionic iodinated contrast material

Table 1

Clinical Characteristics of Patients with Various Tumor Mutations

	Training Set		Testing Set	
Characteristics	*ALK*+	*ALK*−	*ALK*+	*ALK*−
No. of patients	29	30	18	95
Age (y)*	57 (30–80)	70 (42–90)	59 (33–82)	67 (39–90)
Sex				
Male	20	13	6	35
Female	9	17	12	50
Unknown	0	0	0	4
Race				
Eastern descent	29	30	9	47
Western descent	0	0	9	47
Unknown	0	0	0	1
Smoking status				
Smoker	9	9	4	45
Never smoker	14	20	12	42
Unknown	6	1	2	8
Stage				
Operable (≤IIIA)	3	2	5	42
Inoperable (≥IIIB)	26	28	13	51
Unknown	0	0	0	2
Histologic cell type				
Adenocarcinoma	29	29	18	80
Squamous cell carcinoma	0	0	0	5
Unknown	0	1	0	10
Mutation				
KRAS	0	0	0	6
TP53	0	0	0	13
Wild type	0	0	0	41
EGFR	0	30	0	35
Tumor location				
Central	13	7	10	21
Peripheral	16	23	8	74
Pleural tail				
Yes	9	23	3	63
No	20	7	15	32
Pleural effusion				
None	12	20	9	71
Small	6	7	6	18
Moderate	6	2	2	4
Large	5	1	1	2
Age > 60 years				
Yes	7	20	4	59
No	22	10	14	36

Note.—Unless otherwise specified, data are numbers of patients. Twenty-three patients with *ALK*+ disease in the training set were treated with crizotinib for a median of 12.3 months (range, 4.86–49.5 months). Fifteen of these patients experienced progression of disease. Fourteen patients with *ALK*+ disease in the test set were treated with crizotinib for a median of 11.3 months (range, 1.9–40.7 months). Ten of these patients experienced progression of disease. *EGFR* = epidermal growth factor receptor, *KRAS* = V-Ki-ras2 Kirsten rat sarcoma viral oncogene homolog, *TP53* = tumor protein 53.

* Data are medians, with ranges in parentheses.

(350 mg iodine per milliliter) administered intravenously at a rate of 2–4 mL/sec; detector collimation, 1.0–5.0 mm (depending on scanner manufacture); beam pitch, 1.0–5.0; rotation time, 0.5–1.0 second; tube voltage, 120 kVp; and tube current, 100–400 mA with automatic exposure control. Reconstruction thicknesses and intervals were 1.0 or 1.25 mm.

To identify a CT *ALK* radiophenotype, we performed an unbiased screen of 24 a priori defined CT image features, carefully selected to assess various radiographic geographic (location), physiologic, and morphologic aspects of tumors, across each patient's CT study. Two board-certified radiologists (R.L.K. and M.B.G., each with more than 15 years of chest oncologic imaging experience) scored each patient's CT study across each of the 24 CT image traits in consensus. The full description of the image traits is provided in Table E1 (online). The radiologists were blinded to the clinical and pathologic information and molecular phenotype status.

Definition of *ALK* Radiogenomic Biomarker

The derivation and validation of the *ALK* radiogenomic CT biomarker occurred in two phases. The first phase consisted of defining the *ALK* radiogenomic CT status (ARCS) biomarker on a training set. The second phase consisted of a validation step where the ARCS biomarker was then validated in an independent set of patients (Fig 1).

To maximize our ability to discriminate *ALK*+ status, we intentionally designed the training set to contain roughly equal numbers of patients with *ALK*+ and *ALK*− NSCLC (29 patients with *ALK*+ NSCLC vs 30 patients with *ALK*− NSCLC) from a single institution (SNUH). Conversely, the validation test set was specifically constructed to then test the performance of the ARCS biomarker in a population that more faithfully reflected the relatively low prevalence of *ALK*+ tumors in the general population and both the potential demographic and mutational diversity encountered in the general NSCLC population. The test set was accordingly derived from multiple institutions and consisted of patients with *ALK*+ NSCLC (n = 18; eight from SNUH and 10 from MGH) and patients with *ALK*− NSCLC (n = 95; 44 from SNUH, 24 from MGH, and 27 from SHC) and contained *EGFR* mutant, *EGFR* wild-type, *TP53*, and *KRAS* mutant cancers. The study population characteristics are described in Table 1.

To establish a discriminator of *ALK*+ status capable of leveraging molecular, clinical-pathologic, and CT image feature data, we utilized a radiogenomic-based approach that incorporated all 24 CT image and six clinical-pathologic features as inputs to define potential associations with the underlying molecular phenotype. A modified random forest classifier was used to select features (27). Briefly, this algorithm extends the classic random forest method by adding additional permutations, where each run is rerandomized and the importance measure of a variable is scored against all other variables. A detailed description of the algorithm can be obtained in the cited material and the R package (28). Logistic regression was then applied to the outputs of the classifier, resulting in a regression equation that yielded a quantitative score, termed the ARCS score (Fig E1 [online]). An ARCS score was then generated for each patient, representing the overall sum of each selected trait multiplied by its coefficient. The optimum binary cutoff value was established by using receiver operating characteristic analysis. Validation of the ARCS biomarker was then performed on the test set by similarly determining each patient's ARCS score and applying the same cutoff score established in the training set. Diagnostic accuracy was determined for the training, test, and the combined overall data sets. Additionally, subset analyses were performed to evaluate the effect of stage on the performance of the ARCS biomarker.

Definition of Crizotinib Durable Response Imaging Biomarker

We next sought to define an image-based biomarker able to identify patients more likely to experience early progression while receiving crizotinib.

Figure 1

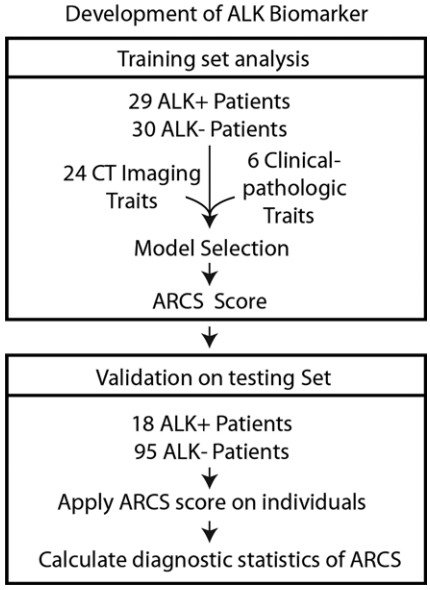

Figure 1: Generation and validation of the ARCS biomarker.

As prespecified by the original crizotinib clinical trials from which these patients were accrued, only patients who completed the full cycle of crizotinib treatment until proven progression or who tolerated the drug without marked toxicity were included in this analysis, yielding 35 patients for subsequent analysis (28). Utilizing the same modified random forest algorithm for trait selection, we trained a binary outcome model including only patients with documented progression (n = 23). The 23 patients were "trained" by assigning them into two groups on the basis of their time to documented progression, in which they had either above or below the median PFS. We then applied the resulting biomarker generated from the modified random forest analysis on the full data set of 35 patients (both censored and noncensored patients) to identify those likely to have a shorter durable response time, with the readers blinded to outcome. Kaplan-Meier survival curves were generated, and the log-rank test was used to assess statistical difference between early PFS versus late PFS groups. Differences in clinical covariates between the two groups of patients defined by the image

biomarker were evaluated by using the Mann-Whitney *U* test.

All statistical analyses were performed with R software, version 3.0.1 *(http://www.R-project.org),* and SPSS, version 15.0 (IBM, Armonk, NY).

Results

Patient Demographic Data, Histologic Subtype, and Molecular Phenotype

The baseline characteristics of the patients are described in Table 1. In total, 172 patients were included in this study. The distribution according to molecular phenotype was as follows: 47 *ALK*+, 65 *EGFR* mutant, 41 *EGFR* wild type, six *KRAS* mutant, and 13 *TP53* mutant.

Development of *ALK* Radiogenomic CT Status Biomarker

Of the 30 total features evaluated, four were ultimately selected in the model as having the strongest predictive ability for *ALK*+ status. Three of the four features were CT image features: central tumor location, large pleural effusion, and the absence of a pleural tail. The fourth feature selected in the model was patient age of less than 60 years. Receiver operating characteristic analysis of the resulting predictor equation scores against actual *ALK*+ status identified an optimal binary cutoff value of −1.115 (range, +7.291 to −3.753), with an area under the curve of 0.846 ($P < .001$) (Fig E1 [online]). Patients with a score of −1.115 or greater were characterized as ARCS+ (Fig 2), whereas patients with a score of less than the cutoff value of −1.115 were characterized as ARCS− (Fig 3).

Measures of Diagnostic Accuracy

Interobserver agreement for scoring the ARCS traits was very good among the two radiologists ($\kappa = 0.82$). The diagnostic accuracy of the ARCS biomarker for *ALK* status classification (*ALK*+ vs *ALK*−) in the training set was 81.4% (48 of 59), with a sensitivity and specificity of 86.2% (25 of 29) and 76.7% (23 of 30), respectively.

Figure 2

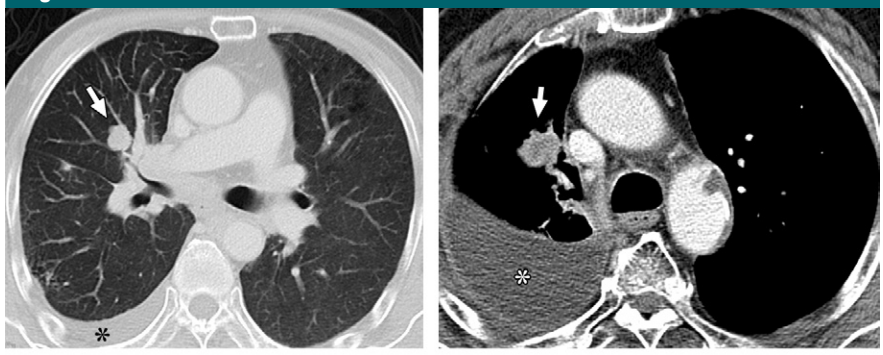

a. b.

Figure 2: Axial CT images in ARCS+ patients with *ALK*+ NSCLC. Images in **(a)** ARCS+ 52-year-old man and **(b)** ARCS+ 75-year-old man with *ALK*+ adenocarcinoma show central tumors (arrow), pleural effusions (*), and absent pleural tails.

Figure 3

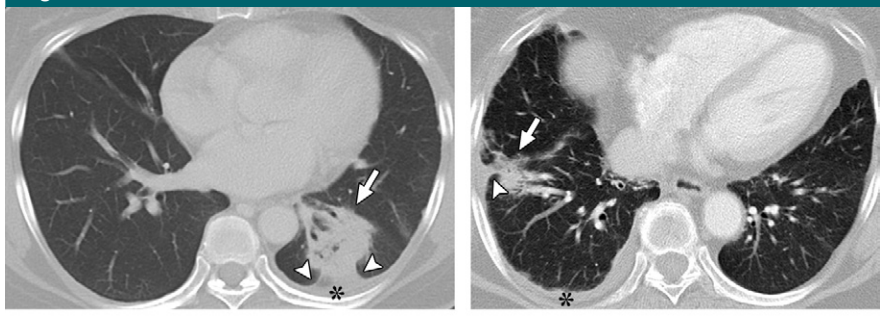

a. b.

Figure 3: Axial CT images in ARCS− patients with *ALK*− NSCLC. **(a)** Image in ARCS− 63-year-old woman with *EGFR* mutant adenocarcinoma shows a peripheral tumor (arrow), pleural tail (arrowheads), and trace pleural effusion (*). **(b)** Image in ARCS− 85-year-old woman with *KRAS* mutant adenocarcinoma shows peripheral tumor (arrow), pleural tail (arrowheads), and a trace left pleural effusion (*).

We next validated the predictive capabilities of the ARCS biomarker in the independent test set by applying the same cutoff value, which revealed a diagnostic accuracy of 78.8% (89 of 113), and sensitivity and specificity of 83.3% (15 of 18) and 77.9% (74 of 95), respectively. Subset analysis of the ARCS biomarker in patients with operable (stage IIIA or lower) disease demonstrated an accuracy, sensitivity, and specificity of 89.4% (42 of 47), 100.0% (five of five), and 88.1% (37 of 42), respectively, versus 73.4% (47 of 64), 76.9% (10 of 13), and 72.5% (37 of 51), respectively, in patients with advanced inoperable (stage IIIB or higher) disease. Overall, the diagnostic accuracy of the ARCS biomarker across the entire study population in predicting *ALK*+ versus *ALK*− NSCLC was 79.7% (137 of 172), with a sensitivity of 85.1% (40 of 47) and a specificity of 77.6% (97 of 125). All results are detailed in Table 2.

Image Biomarker Predicts Durable Treatment Response to Crizotinib in Patients with *ALK*

At the time of our evaluation, 23 of the 35 patients had disease that progressed while they were being treated with crizotinib. The median follow-up time and median PFS for the study cohort were 75 and 11.9 months, respectively. Applying the same inputs of the 30 traits and utilizing the modified random forest variable selection method

Table 2

Diagnostic Accuracy

Subset	Sensitivity (%)	Specificity (%)	Positive Predictive Value (%)	Negative Predictive Value (%)	Accuracy (%)
Training set	86.2 (25/29) [68.3, 96.0]	76.7 (23/30) [57.7, 90.0]	78.1 (25/32) [60.0, 90.7]	85.2 (23/27) [66.3, 95.7]	81.4 (48/59)
Testing set	83.3 (15/18) [58.6, 96.2]	77.9 (74/95) [68.2, 85.8]	41.7 (15/36) [25.5, 59.2]	96.1 (74/77) [89.0, 99.1]	78.8 (89/113)
Operable disease (≤3A)	100 (5/5) [48.0, 100]	88.1 (37/42) [74.4, 96.0]	50.0 (5/10) [18.9, 81.1]	100 (37/37) [90.4, 100]	89.4 (42/47)
Inoperable disease (≥3B)	76.9 (10/13) [46.2, 94.7]	72.5 (37/51) [58.3, 84.1]	41.7 (10/24) [22.1, 63.3]	92.5 (37/40) [79.6, 98.3]	73.4 (47/64)
Overall	85.1 (40/47) [71.7, 93.8]	77.6 (97/125) [69.3, 84.6]	58.8 (40/68) [46.2, 70.6]	93.3 (97/104) [86.6, 97.2]	79.7 (137/172)

Note.—Data in parentheses are raw data, with 95% confidence intervals in brackets.

Figure 4

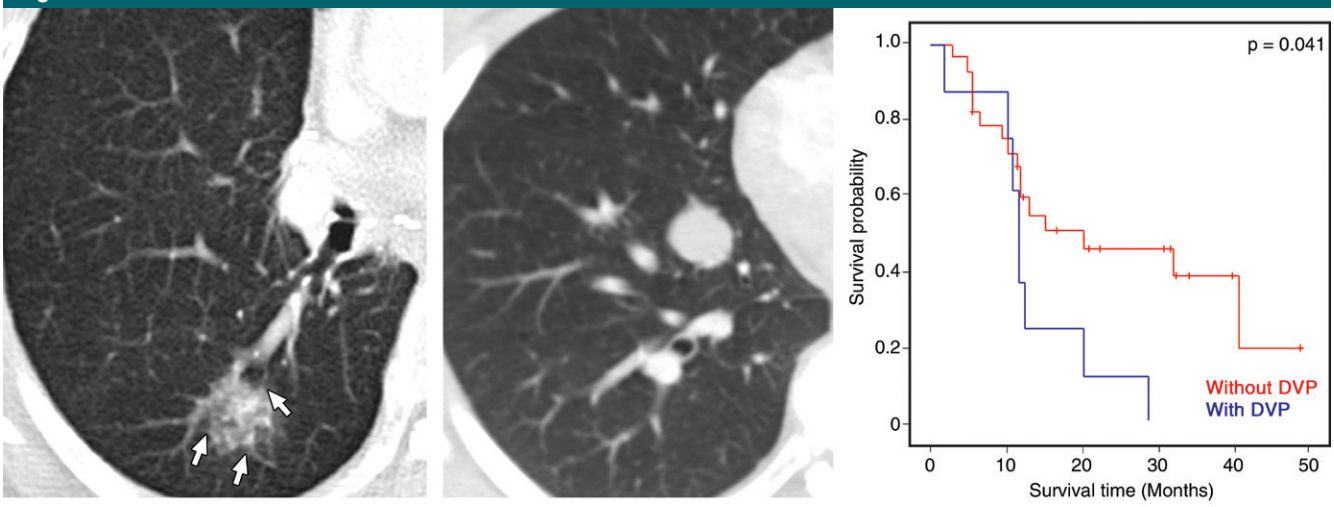

Figure 4: Crizotinib durable response imaging biomarker. **(a)** Axial CT image in 48-year-old man with *ALK*+ adenocarcinoma with the disorganized vascular pattern trait (arrows) and early disease progression (PFS, 4 months). **(b)** Axial CT image in 59-year-old woman with *ALK*+ adenocarcinoma with the absence of the disorganized vascular pattern image trait (PFS, 15 months). **(c)** Graph of Kaplan-Meier survival curve estimates show PFS for patients with and those without the disorganized vascular pattern *(DVP)* image trait.

to identify a potential biomarker that could predict patients likely to experience a shorter durable response time to crizotinib, the model identified a single trait, "disorganized vascular pattern," as a PFS classifier (Fig 4). This durable response image biomarker distinguished patients who had shorter time to progression after initiation of crizotinib therapy, with a median PFS time of 11.4 months in the trait-positive group (early PFS group), compared with 20.2 months in the trait-negative group (late PFS group) (hazard ratio, 2.437; 95% confidence interval: 1.00, 5.85; log-rank $P = .041$) (Fig 4). No statistically significant differences between the trait-positive and trait-negative groups were found in the clinical covariates measured (Table 3).

Discussion

Herein we derive and validate a radiogenomic classifier termed the ARCS biomarker that tracks the *ALK*+ phenotype in NSCLC from CT image data. Our analysis reveals that *ALK*+ tumors have a CT radiophenotype that distinguishes them from tumors with other NSCLC molecular phenotypes (*EGFR* mutant, wild type, *KRAS*, and *TP53*). This radiophenotypic finding is concordant with clinical-pathologic findings that *ALK*+ tumors are mutually exclusive from tumors with *EGFR* or *KRAS* mutations (5,7). Finally, we also discovered an imaging biomarker that can potentially identify patients likely to have shorter durable response to the *ALK* inhibitor crizotinib.

Fluorescence in situ hybridization is the current standard of reference for clinical determination of *ALK*+ status in patients with NSCLC. The purpose of ARCS is not to replace molecular testing but instead to enable radiologists to better understand the distinctive phenotypic imaging findings associated with *ALK*+ tumors and to translate this understanding into clinical practice by allowing radiologists to raise clinical suspicion for this molecular subtype where appropriate,

through deeper utilization of available clinical imaging information. Benefits of ARCS are twofold: *(a)* It is easy to calculate, as evidenced by the strong interobserver reliability, and *(b)* it is obtainable in almost every patient through routine clinical evaluation. Thus, the ARCS biomarker can be applied in almost any clinical setting in which the patient's age at diagnosis is known and where CT imaging is performed for the primary tumor.

The ARCS biomarker was purposely created in a highly enriched *ALK*+ population with advanced disease to optimize signal-to-noise differences between *ALK*+ and *ALK*− tumors. Importantly, the performance of the ARCS biomarker was comparable in the larger independent test set population, which contained fewer patients with *ALK*+ disease as well as a background of other NSCLC mutant subtypes. While subset analysis revealed that ARCS continues to perform well in patients with advanced-stage inoperable disease, the finding that ARCS performs significantly better in patients with early stage, operable disease is intriguing and unexpected. Although no current treatment guidelines yet exist for use of crizotinib in the setting of neoadjuvant therapy, this treatment may be plausible given that it is becoming common practice to use targeted therapy prior to surgery in other cancer types (29,30). Therefore, if future clinical studies do demonstrate a benefit for neoadjuvant treatment of patients with *ALK*+ operable disease, it is feasible that application of ARCS may provide important clinical value in the diagnostic evaluation and molecular characterization of disease in such patients. Although our analysis was performed in a multi-institutional, international study cohort, further verification of these findings in larger, multi-institutional cohorts is warranted.

These data provide optimism regarding the potential role of noninvasive imaging techniques in better understanding phenotype-genotype relationships and in aiding molecular subtype discrimination in solid cancers (3). Interestingly, the three imaging features presented in this model contrast with the conventional imaging presentation of lung adenocarcinomas; specifically, adenocarcinomas traditionally tend to be located peripherally and often present with pleural tails resulting from desmoplastic reactions, whereas we found that *ALK*+ tumors, which are mostly adenocarcinomas by cell type, are often centrally located and without pleural tails (31,32). Further investigation is required, but we posit that the group of radiologically "non-classic" adenocarcinomas may be enriched in these low-prevalence *ALK*+ cancers. As our technique is easily reproducible, these radiogenomic methods should be explored in other cancer types for which imaging is widely available. It is possible that, similar to what we found here, the heterogeneity in the radiographic appearances of other tumors or disease processes—the radiographic "outliers," so to speak—may in fact be explained by underlying differences in molecular phenotype.

In addition to providing a reproducible scoring method for detecting *ALK*+, we also found that tumors with a disorganized vessel phenotype tended to have shorter durable response to crizotinib, the only currently approved therapy for *ALK*+ tumors. Despite the promise of targeted therapy, the efficacies of most molecular inhibitors are 12%–65%, with crizotinib in the high end of the spectrum, with an efficacy of up to 65% (13,23,33). Although resistance mechanisms are starting to be understood, there is currently no viable method to stratify patients who will maximally benefit from this therapy (34). Despite ongoing efforts, biomarker candidates predictive of crizotinib treatment outcome are yet to be identified (35). Such biomarkers are desperately needed to predict treatment efficacy and optimize treatment planning, all of which would be greatly beneficial to patients, particularly if they can be based on their CT findings prior to treatment administration. The disorganized vessel phenotype offers promise as a potential biomarker for segregating short and long durable responders. Although the mechanisms are unknown and additional confirmatory studies are clearly warranted, it is possible that this image biomarker could be related to poor delivery of the drug because the vasculature feeding the tumor is unstructured and permeative. Regardless, this finding is promising, with further characterization and validation of this marker currently underway.

Table 3

Comparison of Covariates in Patients with Crizotinib Response Predictor–Positive Disease with Those in Patients with Crizotinib Response Predictor–Negative Disease

Characteristic	*P* Value
Sex	.525
Race	.525
Smoker	.624
Tumor stage	.624
Age < 60 years	.525
Histology	>.99
Received chemotherapy	.624
Received EGFR inhibitor	.536

Despite the advantages of utilizing a training and independent test cohort for validation, limitations of our analysis merit discussion. First, because our data are retrospective and limited to mostly Eastern Asian and Caucasian populations, care should be taken before generalizing our findings to other populations. Interestingly, the test set was derived from a population of largely Western descent, yet revealed similar sensitivity and specificity to those in the training population, which consisted of patients of East Asian descent. Second, we were not able to validate our crizotinib treatment response biomarker owing to the relatively recent approval of this drug, limiting inclusion of sufficient numbers of patients for an independent validation cohort. Finally, these data do not examine the potential for positron emission tomography/CT–based features that can potentially serve as an alternative method for evaluating

ALK+ status. However, we believe both the findings described herein and the general radiogenomic approach described are robust and scalable.

In summary, *ALK*+ tumors possess a distinctive CT radiophenotype that, when combined with clinical-pathologic characteristics, defines an *ALK*-specific radiogenomic biomarker that can aid in identification of *ALK*+ tumors with reasonably strong accuracy. Furthermore, a CT image biomarker may be able to identify patients likely to derive a durable clinical benefit from crizotinib prior to initiation of targeted therapy, thereby aiding in patient stratification. While these results are promising, both the ARCS and the crizotinib response biomarker ultimately will require further validation in larger cohorts.

Disclosures of Conflicts of Interest: S.Y. No relevant conflicts of interest to disclose. **R.L.K.** Financial activities related to the present article: none to disclose. Financial activities not related to the present article: is the chief medical officer of Imaging Endpoints Core Lab. Other relationships: none to disclose. **R.O.** No relevant conflicts of interest to disclose. **C.M.** No relevant conflicts of interest to disclose. **M.B.G.** No relevant conflicts of interest to disclose. **G.J.W.** Financial activities related to the present article: none to disclose. Financial activities not related to the present article: has received honoraria from Genentech, Eli Lilly, Pfizer, Caris Life Sciences, Quintiles, and Medscape. Other relationships: none to disclose. **A.J.I.** Financial activities related to the present article: none to disclose. Financial activities not related to the present article: is a consultant for Bioreference Laboratories; has a patent for snapshot genotyping with royalties paid to Bioreference Laboratories. Other relationships: none to disclose. **D.W.K.** No relevant conflicts of interest to disclose. **M.D.K.** No relevant conflicts of interest to disclose.

References

1. Camidge DR, Bang YJ, Kwak EL, et al. Activity and safety of crizotinib in patients with ALK-positive non-small-cell lung cancer: updated results from a phase 1 study. Lancet Oncol 2012;13(10):1011–1019.
2. Kosaka T, Yatabe Y, Endoh H, Kuwano H, Takahashi T, Mitsudomi T. Mutations of the epidermal growth factor receptor gene in lung cancer: biological and clinical implications. Cancer Res 2004;64(24):8919–8923.
3. Shaw AT, Yeap BY, Mino-Kenudson M, et al. Clinical features and outcome of patients with non-small-cell lung cancer who harbor EML4-ALK. J Clin Oncol 2009;27(26):4247–4253.
4. Shaw AT, Yeap BY, Solomon BJ, et al. Effect of crizotinib on overall survival in patients with advanced non-small-cell lung cancer harbouring ALK gene rearrangement: a retrospective analysis. Lancet Oncol 2011;12(11):1004–1012.
5. Soda M, Choi YL, Enomoto M, et al. Identification of the transforming EML4-ALK fusion gene in non-small-cell lung cancer. Nature 2007;448(7153):561–566.
6. Mino-Kenudson M, Chirieac LR, Law K, et al. A novel, highly sensitive antibody allows for the routine detection of ALK-rearranged lung adenocarcinomas by standard immunohistochemistry. Clin Cancer Res 2010;16(5):1561–1571.
7. Rodig SJ, Mino-Kenudson M, Dacic S, et al. Unique clinicopathologic features characterize ALK-rearranged lung adenocarcinoma in the western population. Clin Cancer Res 2009;15(16):5216–5223.
8. Camidge DR, Bang Y, Kwak EL, et al. Progression-free survival (PFS) from a phase I study of crizotinib (PF-02341066) in patients with ALK-positive non-small cell lung cancer (NSCLC). J Clin Oncol 2011;29(Suppl):2501.
9. Ou SH, Kwak EL, Siwak-Tapp C, et al. Activity of crizotinib (PF02341066), a dual mesenchymal-epithelial transition (MET) and anaplastic lymphoma kinase (ALK) inhibitor, in a non-small cell lung cancer patient with de novo MET amplification. J Thorac Oncol 2011;6(5):942–946.
10. Paez JG, Jänne PA, Lee JC, et al. EGFR mutations in lung cancer: correlation with clinical response to gefitinib therapy. Science 2004;304(5676):1497–1500.
11. Kwak EL, Bang YJ, Camidge DR, et al. Anaplastic lymphoma kinase inhibition in non-small-cell lung cancer. N Engl J Med 2010;363(18):1693–1703.
12. Karapetis CS, Khambata-Ford S, Jonker DJ, et al. K-ras mutations and benefit from cetuximab in advanced colorectal cancer. N Engl J Med 2008;359(17):1757–1765.
13. Pérez-Soler R, Chachoua A, Hammond LA, et al. Determinants of tumor response and survival with erlotinib in patients with non–small-cell lung cancer. J Clin Oncol 2004;22(16):3238–3247.
14. Kuo MD, Gollub J, Sirlin CB, Ooi C, Chen X. Radiogenomic analysis to identify imaging phenotypes associated with drug response gene expression programs in hepatocellular carcinoma. J Vasc Interv Radiol 2007;18(7):821–831.
15. Segal E, Sirlin CB, Ooi C, et al. Decoding global gene expression programs in liver cancer by noninvasive imaging. Nat Biotechnol 2007;25(6):675–680.
16. Diehn M, Nardini C, Wang DS, et al. Identification of noninvasive imaging surrogates for brain tumor gene-expression modules. Proc Natl Acad Sci U S A 2008;105(13):5213–5218.
17. Gevaert O, Xu J, Hoang CD, et al. Non-small cell lung cancer: identifying prognostic imaging biomarkers by leveraging public gene expression microarray data—methods and preliminary results. Radiology 2012;264(2):387–396.
18. Yamamoto S, Maki DD, Korn RL, Kuo MD. Radiogenomic analysis of breast cancer using MRI: a preliminary study to define the landscape. AJR Am J Roentgenol 2012;199(3):654–663.
19. Jamshidi N, Diehn M, Bredel M, Kuo MD. Illuminating radiogenomic characteristics of glioblastoma multiforme through integration of MR imaging, messenger RNA expression, and DNA copy number variation. Radiology 2014;270(1):1–2.
20. Kuo MD, Jamshidi N. Behind the numbers: decoding molecular phenotypes with radiogenomics—guiding principles and technical considerations. Radiology 2014;270(2):320–325.
21. Lee HJ, Kim YT, Kang CH, et al. Epidermal growth factor receptor mutation in lung adenocarcinomas: relationship with CT characteristics and histologic subtypes. Radiology 2013;268(1):254–264.
22. Kim D, Ahn M, Yang P, et al. Results of a global phase II study with crizotinib in advanced ALK-positive non-small cell lung cancer (NSCLC). J Clin Oncol 2012;30(Suppl):7533.
23. Shaw AT, Kim DW, Nakagawa K, et al. Crizotinib versus chemotherapy in advanced ALK-positive lung cancer. N Engl J Med 2013;368(25):2385–2394.
24. Eisenhauer EA, Therasse P, Bogaerts J, et al. New response evaluation criteria in solid tumours: revised RECIST guideline (version 1.1). Eur J Cancer 2009;45(2):228–247.
25. Brambilla E, Travis WD, Colby TV, Corrin B, Shimosato Y. The new World Health Organization classification of lung tumours. Eur Respir J 2001;18(6):1059–1068.
26. Lynch TJ, Bell DW, Sordella R, et al. Activating mutations in the epidermal growth

factor receptor underlying responsiveness of non-small-cell lung cancer to gefitinib. N Engl J Med 2004;350(21):2129–2139.

27. Kursa MB, Rudnicki WR. Feature selection with the Boruta package. J Stat Softw 2010; 36(11):1–13.

28. Therasse P, Arbuck SG, Eisenhauer EA, et al. New guidelines to evaluate the response to treatment in solid tumors. European Organization for Research and Treatment of Cancer, National Cancer Institute of the United States, National Cancer Institute of Canada. J Natl Cancer Inst 2000;92(3):205–216.

29. Gianni L, Eiermann W, Semiglazov V, et al. Neoadjuvant chemotherapy with trastuzumab followed by adjuvant trastuzumab versus neoadjuvant chemotherapy alone, in patients with HER2-positive locally advanced breast cancer (the NOAH trial): a randomised controlled superiority trial with a parallel HER2-negative cohort. Lancet 2010; 375(9712):377–384.

30. Schaake EE, Kappers I, Codrington HE, et al. Tumor response and toxicity of neoadjuvant erlotinib in patients with early-stage non-small-cell lung cancer. J Clin Oncol 2012; 30(22):2731–2738.

31. Webb WR. The pleural tail sign. Radiology 1978;127(2):309–313.

32. Woodring JH, Stelling CB. Adenocarcinoma of the lung: a tumor with a changing pleomorphic character. AJR Am J Roentgenol 1983;140(4):657–664.

33. Verma S, Miles D, Gianni L, et al. Trastuzumab emtansine for HER2-positive advanced breast cancer. N Engl J Med 2012;367(19):1783–1791. [Published correction appears in N Engl J Med 2013;368(25): 2442.]

34. Choi YL, Soda M, Yamashita Y, et al. EML4-ALK mutations in lung cancer that confer resistance to ALK inhibitors. N Engl J Med 2010;363(18):1734–1739.

35. Park JW, Kerbel RS, Kelloff GJ, et al. Rationale for biomarkers and surrogate end points in mechanism-driven oncology drug development. Clin Cancer Res 2004;10(11): 3885–3896.